Check for updates



Optics Letters

# Uniformly orbitalized beams

Olga Korotkova[1,*] and Sergey A. Ponomarenko[2,3]

[1]Department of Physics, University of Miami, 1320 Campo Sano Avenue, Coral Gables, Florida 33146, USA
[2]Department of Electrical and Computer Engineering, Dalhousie University, Halifax, Nova Scotia, B3J 2X4, Canada
[3]Department of Physics and Atmospheric Science, Dalhousie University, Halifax, Nova Scotia, B3H 4R2, Canada
*korotkova@physics.miami.edu

Received 25 August 2026; revised 3 October 2026; accepted 19 October 2026; posted 20 October 2026; published 3 November 2026

**We show that an incoherent superposition of perfect correlation vortex sources with different OAM indices maintains a uniform degree of orbitalization everywhere outside of the vortex core. In the nearly incoherent source limit, the orbitalization of the beam radiated by such a source remains invariant upon propagation in free space. Moreover, we can control the degree of orbitalization by adjusting weighting coefficients. We further demonstrate that the degree of orbital anisotropy, the OAM concurrence, and the OAM degree of coherence are invariant upon free-space propagation as well.** © 2026 Optica Publishing Group. All rights, including for text and data mining (TDM), Artificial Intelligence (AI) training, and similar technologies, are reserved.

https://doi.org/10.1364/OL.615294

Synthesis of deterministic or random light sources radiating beams with controllable uniform and nonuniform polarization has been a subject of extensive investigations during the last several decades [1–5]. We can generate uniformly elliptically polarized deterministic beams, described by their Jones vectors [1], as well as beams with radial, azimuthal [3], or more complex polarization distributions, which include full Poincaré beams [4] and optical skyrmions [5]. The latter carry nontrivial topological textures due to their inhomogeneous polarization states.

For random vector beams, characterized by $2 \times 2$ polarization matrices [1,2], one can finely tune the spatial distribution of the degree of polarization in addition to its geometry and topology [6]. In free-space propagation, deterministic beams with uniform polarization always preserve this property, while it is not generally true for their partially coherent cousins [7]. However, it still appears possible to maintain polarization invariance of some random beams [6,8]. Overall, we can sculpt the polarization properties of freely propagating beams on demand.

Recently, the counterpart of the polarization theory of vector beams was established for scalar beams carrying Orbital Angular Momentum (OAM) [9] in any number of modes, say $L$ [10–12]. The central objects of this formulation are the $L$-dimensional OAM vector [11] and the $L \times L$ orbitalization matrix (OM) [12] for deterministic and random beams, respectively. The elements of an OAM vector are found from the field as its radially dependent polar Fourier components, while the elements of the OM are pair correlations of such polar Fourier components, which can be filtered out from the beams' cross-spectral density [1].

There are two limiting orbitalization states: complete orbitalization and unorbitalization. Completely orbitalized beams are indistinguishable from deterministic beams. In this limit, the cross-spectral density factors, implying factorization of the OM into the outer product of an OAM vector. The optical field described by this OAM vector then traces an orbitalization ellipse at any given radius [11], which can be viewed as the counterpart of the well-known polarization ellipse [1,2]. In the other limit, completely unorbitalized beams are characterized by diagonal OM matrices with equal elements. For $L = 2$ orbitalization, the polarization properties are uniquely defined and identical in form [13], while for $L > 2$ several quantitative extensions are possible, as for any multidimensional density matrix [14,15]. For example, the degree of orbitalization can be generalized by leveraging rank-based decomposition of the OM [12], or the degree of orbital anisotropy can be deduced as the variance of the OM's eigenvalue distribution with respect to uniform [16]. In addition, access to the full eigenvalue sequence enables the extraction of quantities analogous to the Schmidt number [17], concurrence [18], and entropy [19] from polarization theory [16].

However, no OAM-carrying beams have been found to date that maintain uniform orbital angular momentum, as well as other aforementioned measures, either in the source plane or during propagation. Indeed, for well-known classes of OAM-endowed random beams, such as twisted Gaussian Schell-model beams [20] and $I_l$-Bessel correlated beams [21], the degree of orbitalization was shown to be necessarily nonuniform at the source and not structurally invariant on free-space propagation [13,22]. We define structural invariance as the self-similarity of a given property upon propagation. The aim of this Letter is to illustrate that an incoherent superposition of several Perfect Correlation Vortices (PCVs) [23] yields a uniform degree of orbitalization in the source plane, at least within its wide outer region. Moreover, for a carefully chosen set of parameters, the degree of orbitalization remains practically invariant on free-space propagation. We elucidate the conditions for which the degree of orbital anisotropy and concurrence behave in line with the degree of orbitalization, and complement the analysis by presenting the degree of OAM coherence, a measure quantifying the maximum pair-radius visibility [24]. We note in passing that coherent superpositions of deterministic perfect vortices [25] give rise to completely orbitalized beams in the source plane. However, the spatial distribution of orbitalization for such deterministic vortex beams rapidly becomes

nonuniform upon free-space propagation away from the source, limiting their practical utility.

We begin by briefly reviewing orbitalization metrics of random, structured beams. Consider cross-spectral density $W(\mathbf{r}_1, \mathbf{r}_2)$ of a scalar, wide-stationary beam where $\mathbf{r}_j = \rho_j \hat{\rho} + \phi_j \hat{\phi} + z\hat{z}$, $j = 1, 2$ [1]. Based on it, the coherence-OAM matrix $\overleftrightarrow{W}(\rho_1, \rho_2, z)$ was introduced for characterization of self- and joint radial pair correlations among the OAM modes composing the beam. Its elements are defined by the expressions [10]

$$W_{lm}^{(OAM)}(\rho_1, \rho_2, z) = \frac{1}{4\pi^2} \int_0^{2\pi} \int_0^{2\pi} W(\mathbf{r}_1, \mathbf{r}_2) e^{i(l\phi_1 - m\phi_2)} d\phi_1 d\phi_2, \tag{1}$$

with topological charges $l, m \in \mathcal{L} \in \mathbb{Z}$, at a pair of radii $\rho_1, \rho_2 \geq 0$ at the transverse beam cross-section specified by $z \geq 0$. For convenience, we will use vectors $\boldsymbol{\xi}_j = \rho_j \hat{\rho} + z\hat{z}$ and confine the discussion to finite-dimensional matrices. To assess various single-radius measures, we define the OM as [12]

$$\overrightarrow{O}(\boldsymbol{\xi}) = \overleftrightarrow{W}(\boldsymbol{\xi}, \boldsymbol{\xi}). \tag{2}$$

In form, it can be regarded as the OAM counterpart of a polarization matrix [1]. As any multidimensional density matrix, it enjoys a number of useful decompositions [14,15]. In particular, it is positive semi-definite, which enables the eigenmode decomposition [12]

$$\overrightarrow{O}(\boldsymbol{\xi}) = \sum_{l=1}^{L} \lambda_l(\boldsymbol{\xi}) \overleftrightarrow{\psi}_l(\boldsymbol{\xi}), \quad \overleftrightarrow{\psi}_l(\boldsymbol{\xi}) = \vec{u}_l(\boldsymbol{\xi}) \vec{u}_l^{\dagger}(\boldsymbol{\xi}), \tag{3}$$

where $\overleftrightarrow{\psi}_l(\boldsymbol{\xi})$ are rank-1 matrices, $\lambda_l(\boldsymbol{\xi}) \geq 0$ are the eigenvalues, and $\vec{u}_l(\boldsymbol{\xi})$ are the eigenvectors, with the dagger denoting the Hermitian adjoint. We will use the normalization

$$\sigma_l(\boldsymbol{\xi}) = \lambda_l(\boldsymbol{\xi}) \Big/ \sum_{n=1}^{L} \lambda_n(\boldsymbol{\xi}), \quad \sum_{l=1}^{L} \sigma_l(\boldsymbol{\xi}) = 1, \tag{4}$$

and assume ordering $\sigma_l(\boldsymbol{\xi}) \geq \sigma_m(\boldsymbol{\xi})$ for $l \leq m$ hereafter.

To assess contributions from the individual OAM modes to their sum, we will quantify the single-radii properties of a modal beam by the following measures. The radial spectral density is defined by the expression [12]

$$S(\boldsymbol{\xi}) = \sum_{l=1}^{L} \lambda_l(\boldsymbol{\xi}), \tag{5}$$

and provides the information about beams' spectral density at a given radius, integrated over the angular variable $\phi$.

The degree of orbitalization is defined as the ratio of the radial intensities in the completely orbitalized state and in the total beam [12]. For two or three modes, it is identical in form to the degree of polarization of an electromagnetic field with two or three spatial components [1,26]. It can be expressed as the normalized spectral gap [16]

$$\mathrm{O}(\boldsymbol{\xi}) = \sigma_1(\boldsymbol{\xi}) - \sigma_2(\boldsymbol{\xi}). \tag{6}$$

Further, the degree of OAM anisotropy for an $L \times L$ OM is defined as the deviation of its spectrum from the uniform distribution [16]. It can be expressed via the OM's eigenvalues as

$$Q^2(\boldsymbol{\xi}) = \frac{1}{L-1} \left[ L \sum_{l=1}^{L} \sigma_l^2(\boldsymbol{\xi}) - 1 \right]. \tag{7}$$

The OAM anisotropy is analogous to the degree of polarization [1] and the degree of polarimetric purity [14,17] for 2D and 3D polarization cases. The OAM concurrence for an $L \times L$ OM, being the generalization of that for bipartite systems [18] to $L$ dimensions, is defined as [16]

$$C^2(\boldsymbol{\xi}) = \frac{L}{L-1} \left[ 1 - \sum_{l=1}^{L} \sigma_l^2(\boldsymbol{\xi}) \right] = 1 - Q^2(\boldsymbol{\xi}). \tag{8}$$

We now invoke the OAM Degree of Coherence (DOC) as the measure of radial-only interference of OAM modes [24]

$$\mu_{OAM}^2(\boldsymbol{\xi}_1, \boldsymbol{\xi}_2) = \frac{\mathrm{Tr}[\overleftrightarrow{W}^{\dagger}(\boldsymbol{\xi}_1, \boldsymbol{\xi}_2) \overleftrightarrow{W}(\boldsymbol{\xi}_1, \boldsymbol{\xi}_2)]}{\prod_{n=1,2} \mathrm{Tr} \overleftrightarrow{W}(\boldsymbol{\xi}_n, \boldsymbol{\xi}_n)}, \tag{9}$$

where Tr denotes the trace. This quantity is identical in form with the electromagnetic DOC, being a suitably normalized Frobenius norm of a $2 \times 2$ or $2 \times 3$ cross-spectral density matrix [27].

Let us now show that uncorrelated superpositions of recently introduced perfect correlation vortices (PCV) [23] in the low-coherence source limit can give rise to (nearly) uniformly orbitalized beams, i.e., those with constant $O(\boldsymbol{\xi})$. In the low-coherence limit of a PCV, we can distinguish two widely separated transverse scales: the source coherence width $\sigma_c$ and an effective width $\sigma_{\mathrm{eff}} = \sqrt{\sigma_c w_0}$, where $w_0$ is the rms width of the source. The low-coherence regime establishes the following hierarchy of spatial scales:

$$\sigma_c \ll \sigma_{\mathrm{eff}} \ll w_0, \tag{10}$$

and $\sigma_{\mathrm{eff}}$ sets an effective longitudinal diffraction length, $z_D = k\sigma_{\mathrm{eff}}^2$. To better grasp the salient features of nearly incoherent PCVs, we introduce the scaling:

$$\overline{\rho}_1 = \rho_1 / \sigma_{\mathrm{eff}}, \qquad \overline{\rho}_2 = \rho_2 / \sigma_{\mathrm{eff}}, \tag{11}$$

and cast Eq. (12) of Ref. [23] for the cross-spectral density of a scalar PCV beam in any transverse plane $z = const$ to the form:

$$W_l(\overline{\boldsymbol{\xi}}_1, \overline{\boldsymbol{\xi}}_2, \phi_1, \phi_2) \propto R_l(\overline{\boldsymbol{\xi}}_1, \overline{\boldsymbol{\xi}}_2) e^{il(\phi_1 - \phi_2)}, \tag{12}$$

where

$$R_l(\overline{\boldsymbol{\xi}}_1, \overline{\boldsymbol{\xi}}_2) = \frac{1}{1 + z^2/z_D^2} \exp\left[ \frac{i\varepsilon(\overline{\rho}_2^2 - \overline{\rho}_1^2)}{2(z/z_R + \varepsilon^2 z_R/z)} \right] \times \exp\left[ -\frac{\varepsilon(\overline{\rho}_1^2 + \overline{\rho}_2^2)}{2(1 + z^2/z_R^2)(1 + z^2/z_D^2)} \right] \times \exp\left[ -\frac{\overline{\rho}_1^2 + \overline{\rho}_2^2}{4\varepsilon(1 + z^2/z_D^2)} \right] I_l\left[ \frac{\overline{\rho}_1 \overline{\rho}_2}{2\varepsilon(1 + z^2/z_D^2)} \right], \tag{13}$$

$z_R = kw_0^2 \gg z_D$ is a Rayleigh range associated with the source width, $I_l(x)$ is a modified Bessel function of order $l$, and $\overline{\boldsymbol{\xi}}_j = \overline{\rho}_j \hat{\rho} + z\hat{z}$, $j = 1, 2$. Further, $\varepsilon = \sigma_c / w_0 \ll 1$ is a small dimensionless parameter of the system in the low-coherence limit. Note that Eq. (12) is exact within the paraxial approximation. We can infer from Eq. (12) that outside a very narrow region of size $\sigma_c \ll w_0$ around the vortex core $\rho = 0$, the intensity profile is quasi-homogeneous, while the (classic) DOC [1] is sharply peaked around a narrow ring centered at $\overline{\rho}_1 = \overline{\rho}_2$ [23].

To demonstrate this, we notice that outside the said narrow range, we can approximate the modified Bessel function of a large argument with an exponential [28], such that $I_l(x) \simeq e^x / \sqrt{x}$

$\forall l$, if $|x| >> |l|^2$. It follows that Eq. (13) reduces to

$$\widetilde{R}_l(\overline{\xi}_1, \overline{\xi}_2) \propto \frac{\varepsilon}{\overline{\rho}_1 \overline{\rho}_2 \sqrt{1 + z^2/z_D^2}} \exp\left[\frac{i\varepsilon(\overline{\rho}_2^2 - \overline{\rho}_1^2)}{2(z/z_R + \varepsilon^2 z_R/z)}\right] \times \exp\left[-\frac{\varepsilon(\overline{\rho}_1^2 + \overline{\rho}_2^2)}{2(1 + z^2/z_D^2)}\right] \exp\left[-\frac{(\overline{\rho}_1 - \overline{\rho}_2)^2}{4\varepsilon(1 + z^2/z_D^2)}\right], \quad (14)$$

i.e., being independent of $l$, $\widetilde{R}_l = \widetilde{R}$. Here we replaced the factor $1 + z^2/z_R^2$ with unity in the second exponential on the right-hand side because we are interested in the PCV evolution over several characteristic diffraction lengths $z_D$ and $z_D \ll z_R$. The magnitude of the cross-spectral density of Eq. (14) corresponds to a quasi-homogeneous source [1] because $|\widetilde{R}_l(\overline{\rho}_1, \overline{\rho}_2, z)| \propto F[\varepsilon(\overline{\rho}_1 + \overline{\rho}_2)/2] G[(\overline{\rho}_1 - \overline{\rho}_2)/\varepsilon]$, where $F$ ($G$) is a slowly (rapidly) varying function of its variables.

Next, we consider an uncorrelated superposition of $L$ PCVs in Eq. (12) with different topological charges $l$:

$$W(\overline{\xi}_1, \overline{\xi}_2, \phi_1, \phi_2) = \sum_{l=1}^{L} \omega_l W_l(\overline{\xi}_1, \overline{\xi}_2, \phi_1, \phi_2), \quad (15)$$

where $\omega_l$ are nonnegative factors (weights). The COAM matrix of such a superposition is diagonal, with the elements:

$$W_{ll}^{(OAM)}(\overline{\xi}_1, \overline{\xi}_2) = \omega_l R_l(\overline{\xi}_1, \overline{\xi}_2). \quad (16)$$

Further, in the low-coherence regime $\varepsilon \ll 1$ ($\sigma_c \ll w_0$), Eqs. (12), (14), and (15) yield

$$W(\overline{\xi}_1, \overline{\xi}_2, \phi_1, \phi_2) \approx \widetilde{R}(\overline{\xi}_1, \overline{\xi}_2) \sum_{l=1}^{L} \omega_l e^{il(\phi_1 - \phi_2)}. \quad (17)$$

Moreover, in this limit, all elements of the COAM matrix become identical, $W_{ll}^{(OAM)} = W^{(OAM)}$, and their free-space diffraction remains negligible. This results in the degree of orbitalization of the form

$$O(\overline{\xi}) = (\omega_{\max,1} - \omega_{\max,2}) \Big/ \sum_{l=1}^{L} \omega_l, \quad (18)$$

where $\omega_{\max,1}$ and $\omega_{\max,2}$ are the largest and the second largest weights. In particular, for a two-mode case with $\omega_{\max,1} = \omega_{\max,2}$, uniform unorbitalization is achieved. Similarly, $Q(\overline{\xi})$ and $C(\overline{\xi})$ can be evaluated to produce constant values depending on the weighting sequence.

We now illustrate our theoretical results with numerical simulations using Eqs. (12), (13), and (15) that quantitatively describe the beam's behavior inside and outside the vortex core. All numerical examples use parameters $\lambda = 633$ nm, $w_0 = 2$ cm, and $\sigma_c = 2$ mm, and we show all figures using dimensional variables (no scaling). Figure 1 illustrates the radial spectral density $S(\boldsymbol{\xi})$, normalized by its maximum value, the degree of orbitalization $O(\boldsymbol{\xi})$, the degree of OAM anisotropy $Q(\boldsymbol{\xi})$, and the OAM concurrence $C(\boldsymbol{\xi})$ of a beam composed of a pair of modes $l \in \{1, 2\}$ with equal weights, $\omega_1 = \omega_2 = 1$. The color density plots are superposed by 19 contours equally spaced in the interval $[0, 1]$, separating 20 regions with different values. In Fig. 1(A) the beam's radial spectral density $S(\boldsymbol{\xi})$ is shown to maintain a remarkable directionality with growing $z$, which may be enhanced even further by adjusting $w_0$ and $\sigma_c$. In this case, $O(\boldsymbol{\xi})$ in Fig. 1(B) and $Q(\boldsymbol{\xi})$ in Fig. 1(C) have very similar distributions: nearly orbitalized (highly anisotropic) in the core and almost unorbitalized (isotropic) in the wide outskirts region in which the beam retains substantial levels of radial spectral density. Figure 1(D) shows the reciprocal trend and

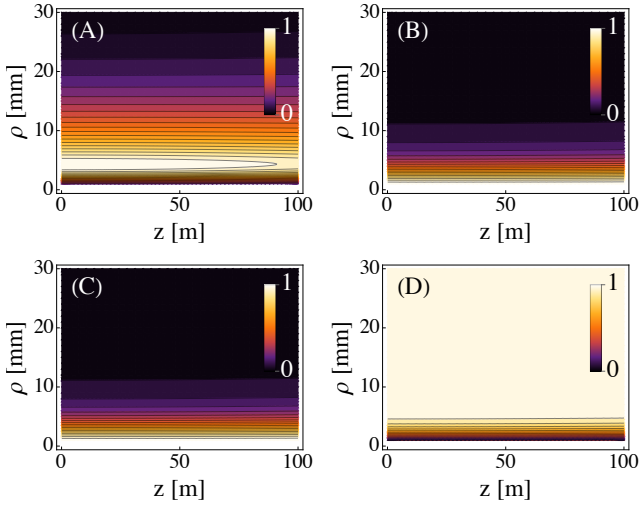


**Fig. 1.** Two equally weighed OAM modes, $l = 1, 2$: (A) normalized spectral density $S(\rho, z)$; (B) degree of orbitalization $O(\rho, z)$; (C) degree of OAM anisotropy $Q(\rho, z)$; and (D) OAM concurrence $C(\rho, z)$.

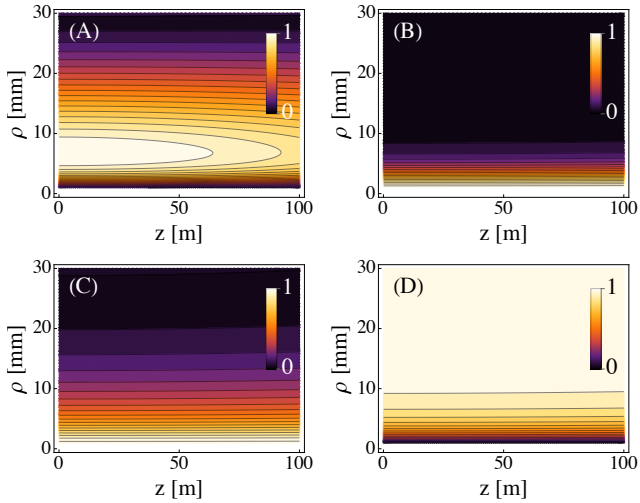


**Fig. 2.** Same as Fig. 1 but for equally weighted ten OAM modes, $l = 1, \ldots, 10$.

changes somewhat more abruptly with the $\rho$ distribution in concurrence with $C(\boldsymbol{\xi})$, having low values in the core and high values outside. This discussion does not include the very narrow region along the beam axis with nearly trivial radial spectral density.

Figure 2 has the same structure as Fig. 1 but uses modes $l \in \{1, \ldots, 10\}$ with equal weights, $\omega_l = 1$. In this case, the beam becomes wider and less directional. Nevertheless, $O(\boldsymbol{\xi})$, $Q(\boldsymbol{\xi})$ and $C(\boldsymbol{\xi})$ remain invariant on propagation. In particular, $O(\boldsymbol{\xi})$ shows much sharper transition to unorbitalized limit outside of the core region, while $Q(\boldsymbol{\xi})$, on the opposite, has a very mild decay in values towards the beam tail. Concurrence $C(\boldsymbol{\xi})$ also sharply transitions from low to very high values towards the beam tail. It is to be noted that, unlike in the 2-mode case in Fig. 1, a much better unorbitalization regime can be attained, in terms of both low absolute values of $O(\boldsymbol{\xi})$ and transition speed from the beam's core to its tails.

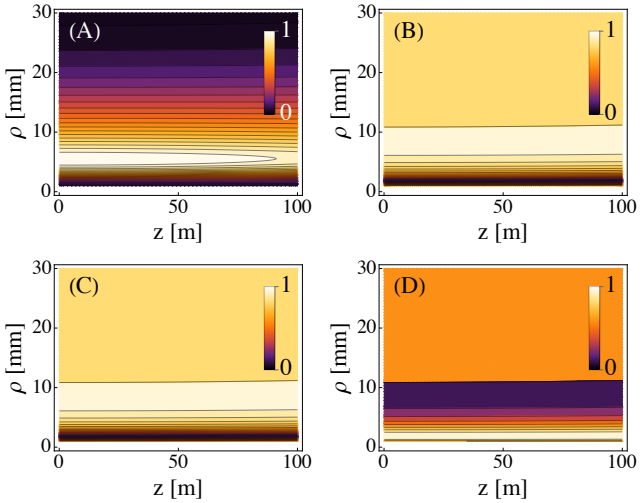


**Fig. 3.** Same as Fig. 1 but for two OAM modes with unequal weights.

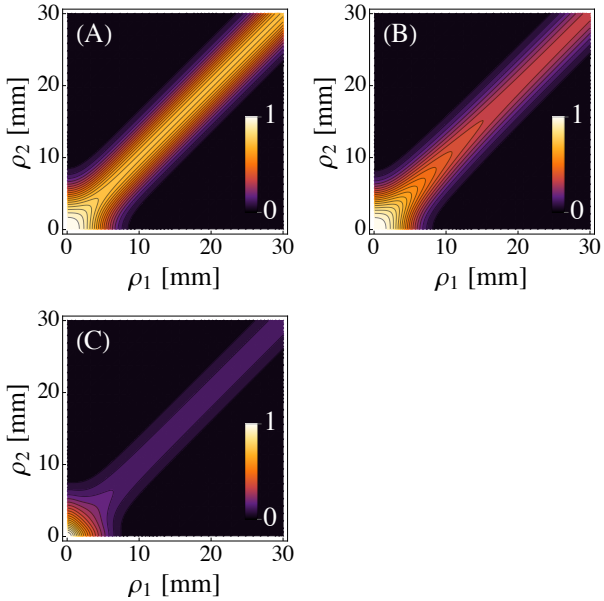


**Fig. 4.** OAM DOC $\mu_{OAM}(\rho_1, \rho_2, 0)$ for sources in (A) Fig. 1, (B) Fig. 2, and (C) Fig. 3.

Figure 3 shows the behavior of a similarly structured beam as in Fig. 1, except that we take the weights $\omega_1 = 1$ for $l = 1$ and $\omega_2 = 10$ for $l = 2$. Here, we demonstrate that by adjusting the modal weights, we can attain any desired values of $O(\boldsymbol{\xi})$, $Q(\boldsymbol{\xi})$ and $C(\boldsymbol{\xi})$ with all quantities remaining (nearly) invariant upon propagation. We note, however, that in this case, the radial behavior of these quantities within the core is more complex, due to the competition among the $I_l$-Bessel functions of different orders.

Figure 4 illustrates the distribution of the OAM DOC $\mu_{OAM}(\boldsymbol{\xi}_1, \boldsymbol{\xi}_2)$, given in Eq. (9), at the source plane, $z = 0$, for sources in Figs. 1–3, as a combination of color-density and contour plot. The same 19-contour/20-region setup is used as in Figs. 1–3. As expected, the value of OAM DOC attains unity only for $\rho_1 = \rho_2 = 0$ and is higher in the region where $\rho_1 \approx \rho_2$. For $z \in [0, 100\ \text{m}]$, the OAM DOC remains virtually invariant in this interval (not shown, as the plots are visually identical at any fixed $z$). This property, in turn, ensures nearly perfect invariance of the orbitalization metrics of the propagating beam.

In summary, we have shown that incoherent superpositions of perfect correlation vortices generated by nearly incoherent sources are uniformly orbitalized outside the vortex core region, maintaining their degree of orbitalization upon free-space propagation. We have also explored the behavior of the degree of orbital anisotropy, the OAM concurrence, and the OAM degree of coherence of such beams and demonstrated their invariance upon propagation. Our results illustrate the possibility of engineering random light sources and beams with uniform orbitalization, including completely unorbitalized beams. We expect our work to inform future research into light beam orbitalization and to facilitate the application of such OAM-carrying beams in optical communications.

**Funding.** Natural Sciences and Engineering Research Council of Canada (RGPIN-2025-04064).

**Disclosures.** The authors declare no conflicts of interest.

**Data availability.** The data underlying the results may be obtained from the corresponding author upon a reasonable request.

## REFERENCES

1. L. Mandel and E. Wolf, *Optical Coherence and Quantum Optics* (Cambridge University Press, 1995).
2. J. Gil and R. Ossikovski, *Polarized Light and the Mueller Matrix Approach* (CRC Press, 2016).
3. Q. Zhan, Adv. Opt. Photon. **1**, 1 (2009).
4. A. M. Beckley, T. G. Brown, and M. A. Alonso, Opt. Express **18**, 10777 (2010).
5. Y. Shen, Q. Zhang, P. Shi, *et al.*, Nat. Photon. **18**, 15 (2024).
6. F. Gori, M. Santarsiero, G. Piquero, *et al.*, J. Opt. A **3**, 1 (2001).
7. D. F. V. James, J. Opt. Soc. Am. A **11**, 641 (1994).
8. E. Wolf, Opt. Lett. **32**, 3400 (2007).
9. L. Allen, M. W. Beijersbergen, R. J. C. Spreeuw, *et al.*, Phys. Rev. A **45**, 8185 (1992).
10. O. Korotkova and G. Gbur, Phys. Rev. A **103**, 023529 (2021).
11. O. Korotkova, Opt. Lett. **50**, 391 (2025).
12. O. Korotkova, J. Opt. **27**, 065606 (2025).
13. S. Martinez, S. Pokharel, and O. Korotkova, Opt. Lett. **49**, 5941 (2024).
14. J. C. Samson, Geophys. J. R. Astron. Soc. **34**, 403 (1973).
15. M. A. Alonso, Adv. Opt. Photon. **15**, 176 (2023).
16. J. Laatikainen, S. Pokharel, and O. Korotkova, "Hanbury Brown–Twiss effect and classical entanglement with OAM-carrying light," arXiv (2026).
17. X. F. Qian and J. H. Eberly, Opt. Lett. **36**, 4110 (2011).
18. M. McLaren, T. Konrad, and A. Forbes, Phys. Rev. A **92**, 023833 (2015).
19. P. Réfrégier, G. Goudail, P. Chavel, *et al.*, J. Opt. Soc. Am. A **21**, 2124 (2004).
20. R. Simon and N. Mukunda, J. Opt. Soc. Am **10**, 95 (1993).
21. S. A. Ponomarenko, J. Opt. Soc. Am. A **18**, 150 (2001).
22. S. Pokharel and O. Korotkova, Opt. Commun. **608**, 133087 (2026).
23. X. Li, S. Bashiri, Y. Ma, *et al.*, Opt. Lett. **49**, 4717 (2024).
24. O. Korotkova and S. Pokharel, Opt. Lett. **49**, 5103 (2024).
25. A. S. Ostrovsky, C. Rickenstorff-Parrao, and V. Arrizón, Opt. Lett. **38**, 534 (2013).
26. J. Ellis, A. Dogariu, S. A. Ponomarenko, *et al.*, Opt. Commun. **248**, 333 (2005).
27. A. T. Friberg and T. Setälä, J. Opt. Soc. Am. A **33**, 2431 (2016).
28. G. Arfken, *Mathematical Methods for Physicists*, 2nd ed. (Academic Press, 1970).